Chapter 7

Study of Refraction Effects for Propagation over Terrain

Vladimir Schejbal, Ondrej Fiser and Vadim Zavodny

Abstract

This chapter investigates the radio-wave propagation above irregular ground, including the troposphere, using physical optics computation. We briefly describe used simplifications, which substantially reduce numerical simulations. Using the principle of stationary phase, we can approximate the propagation over a terrain (the PO approximation of the vector problem with a 3-D surface) with a 2-D surface. Moreover, we approximate the reflection coefficient for a surface with random deviations considering the surface standard deviation and the local Fresnel reflection coefficient for the smooth ground. We present the novel computations of physical optics for investigations of radar coverage diagrams. We consider both monostatic and bistatic radars, the far-field antenna measuring ranges, and studies of air refraction index. We validate the calculations by both experimental results and the other numerical simulations. The experimental results changed during seasons and according to terrain and troposphere conditions including vegetation, cultivation, snow, and air temperature and pressure.

Keywords: electromagnetic propagation, electromagnetic reflection, microwave propagation, losses, radar antennas, electromagnetic refraction

1. Introduction

Propagation of radio waves above earth is very challenging for uncountable communication tasks comprising the radar coverage and far-field antenna measurement ranges. Several methods have been described [1–13] such as geometrical optics (GO) and various modifications of the geometrical theory of diffraction. Full wave methods are rather demanding, bearing in mind the memory and central processing unit (CPU).

We present a brief description of the physical optics (PO) method [14–22] applied for irregular ground reflection considering both horizontal and vertical polarizations, electrical properties of earth (i.e., reflection coefficient), scattering of radio waves from random surfaces, and the shadow radiation. The improved computation of radio waves above uneven ground uses PO and line integrals, taking into consideration the vector problem and shadowing [18, 19]. This is a more consistent method for low-altitude fields and diffraction zones without any additional alternatives.

We perform new numerical simulations, which we compare with ample experimental results and other numerical simulations such as the parabolic equation method (PEM) for altered environment circumstances and modifications.

The evolutionary processes are also discussed and are fully referenced below. We investigate radar coverage diagrams including monostatic and bistatic radars, far-field measuring range of antenna with separation roughly 1 km, and troposphere refraction effects for separation of 49.8 km. The longstanding testing demonstrates that the PO could present reliable computations for low heights and diffraction zones for numerous irregular grounds and real distribution of refraction.

2. Computation of irregular ground reflection

Based on the PO method [3, 4], the computation of irregular ground reflection was derived [14]. However in the 1970s, it was necessary to diminish memory and CPU time. Therefore using a stationary phase method, the line integrals were computed instead of surface integrals, and scalar solutions were only employed. The earliest method has been progressively enlarged. Gradually, we have included various options considering both horizontal and vertical polarizations, electrical properties of earth (i.e., reflection coefficient), the scattering of radio waves from random surfaces, and the shadow radiation. Considering Ufimtsev's results [23–25] a totally new approach to analyze propagation over irregular terrain could be used. The improved computation of radio waves above uneven ground uses PO and line integrals and takes into consideration the vector problem and shadowing [18, 19]. That is a more consistent method for low-altitude fields and diffraction zones without any additional alternatives.

The PO method analyzes an antenna A above the ground as is displayed in **Figure 1**. The sum of incident, $\boldsymbol{E}_i(\mathrm{P})$, and scattered, $\boldsymbol{E}_s(\mathrm{P})$, electric fields could be used everywhere for calculation of the resultant field. The vector of the total electric field, $\boldsymbol{E}(\mathrm{P})$, at point P is

$$\boldsymbol{E}(\mathrm{P}) = \boldsymbol{E}_i(\mathrm{P}) + \boldsymbol{E}_s(\mathrm{P}). \tag{1}$$

The $\boldsymbol{E}_i(\mathrm{P})$ field may be calculated as a spherical wave. An actual scattered body is substituted by the corresponding currents induced on its surface; that is, an allocation of corresponding currents in free space should be computed, which transmit without restriction in all paths. If these currents were computed exactly, they would deliver the accurate scattering results.

Radio-wave scattering by certain impenetrable bodies with local reflection coefficients can be computed using PO [23–25]. According to **Figure 1** the earth's surface may be separated into illuminated, S_{il}, and shadowed, S_{sh}, parts with a shadow curve between them.

According to [3] the GO is a limiting form of the PO. The spread border of the shadow in the diffraction phenomena becomes the sharp shadow of GO as the

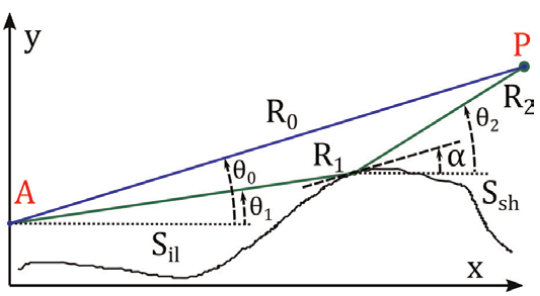

Figure 1.
Propagation geometry.

wavelength tends to zero. Therefore both GO and PO are very useful in the analyses of microwave propagation. Bearing in mind the PO, body surface fields are calculated using the GO. Therefore, the induced sources are only defined on the S_{il} of the scattering object. The components of the S_{sh} are set to zero.

The propagation above the earth (i.e., the PO calculation of the vector problem with 3-D surface) may be substantially reduced, both from memory and CPU time points of view. Using the principle of stationary phase [26]

$$\int_{-\infty}^{\infty} \exp\left(-j\pi z^2/2\right)dz = \sqrt{2}\exp\left(-j\pi/4\right) \tag{2}$$

where the horizontal polarization component E_{sz}(P) and the maximum value of the incident electric vector E_0 at a distance R_0 are [14]

$$\frac{E_{sz}(P)}{|E_0|} = \frac{R_0 e^{j\pi/4}}{2\sqrt{\lambda}} \int_a^b f(\theta_1)\left[(1-\Gamma)\sin(\theta_1-\alpha) + (1+\Gamma)\times\sin(\theta_2-\alpha)\right] \frac{e^{-jk(R_1+R_2-R_0)}}{\sqrt{R_1R_2(R_1+R_2)}} \frac{dx}{\cos\alpha} \tag{3}$$

where R_0, R_1, R_2, θ_1, θ_2, and α are shown in **Figure 1**, $f(\theta_1)$ is the normalized antenna radiation pattern with phase center at point A at height h_A over the terrain, Γ is the Fresnel reflection coefficient (local reflection coefficient), $k = 2\pi/\lambda$, λ is the wavelength, and a, b are limits of the illuminated part S_{il}. A similar equation can be derived for vertical polarization using H_{sz} [15]. Therefore, this method takes into account the polarization. A rather analogous approach is used in [9].

The reflection coefficient for a surface with random deviations could be approximated by

$$\Gamma = \Gamma_0 \ \exp.\left[-2(2\pi\sigma\ \sin\ \gamma_0/\lambda)^2\right] \tag{4}$$

where σ is the surface standard deviation, Γ_0 is the local Fresnel reflection coefficient for the smooth surface for the horizontal (or vertical) polarization, and γ_0 is the grazing (reflection) angle—the angle between the tangent and the incident (reflected) ray. Obviously, better models were proposed [4, 5, 11] considering surfaces as random processes. However, they are rather complicated, and selection of parameters such as correlation length could be questionable.

The improved computations [18, 19] of scattered fields consider the reflected radiation component, E_{sz}^{ref}, (with the reflection coefficient Γ terms) and the shadow radiation component, E_{sz}^{sh}:

$$S_{sz}^{ref}(P) = \frac{|E_0|R_0 e^{j\pi/4}}{2\sqrt{\lambda}} \int_a^b f(\theta_1)\Gamma[\sin(\theta_2-\alpha) - \sin(\theta_1-\alpha)] \times \frac{e^{-jk(R_1+R_2-R_0)}}{\sqrt{R_1R_2(R_1+R_2)}} \frac{dx}{\cos\alpha} \tag{5}$$

$$S_{sz}^{sh}(P) = \frac{|E_0|R_0 e^{j\pi/4}}{2\sqrt{\lambda}} \int_a^b f(\theta_1)[\sin(\theta_2-\alpha) + \sin(\theta_1-\alpha)] \times \frac{e^{-jk(R_1+R_2-R_0)}}{\sqrt{R_1R_2(R_1+R_2)}} \frac{dx}{\cos\alpha} \tag{6}$$

Similar equations may be obtained for vertical polarization utilizing the H magnetic field. Thus, the PO method respects the polarization.

The reflected component depends on the local reflection coefficient, Γ, considering the surface standard deviation, σ. On the other hand, the shadow-emitted power corresponds to the entire power incident on a scattered body, and it is not

determined by the reflection coefficients. Considering the shadow contour theorem, it is not determined by the structure of the scattered body and is completely influenced only by the dimensions and the shape of the shadow line. For the shadow sector, at a limited extent from the scattered body (at the rear of body), the shadow emission for a very short wavelength can be counted as an electromagnetic wave beam. This beam approximately cancels the incident field, and the reflected beams nearly disappear. The shadow radiation gives origin to edge waves, creeping waves, and surface diffracted rays.

The previous computations of low-altitude propagation (LAP) and transient zone (TZ) [16] use the knife-edge diffraction [1] and Fock's spherical surface solution [5]. Both are scalar solutions, which neglect terrain imperfections. These methods are well known and have been extensively used. They have been proven as very efficient approximate methods for real terrain both analytically and experimentally. The transient zone would be considered, if the differences between the reflected and incident rays were less than a third of the wavelength. The low altitude would be considered, if the differences were less than $\lambda/2\pi$. Therefore the previous computations are relatively artificial as two quite different approximations are used for the computation, and the transient zone limits are only supported by an ad hoc assumption.

The comparison [18, 19] of the previous and new methods shows that the improved analysis of propagation over irregular terrain could be much more useful and accurate. Thus, Eqs. (5) and (6) may be employed for computation of both illuminated and shadow radiation. The calculation may be performed for greater heights (greater differentiations between incident and reflecting beams) together with lower heights (i.e., it is not required to compute the low heights and some transient regions). This offers much more consistent results, which consider the polarization even for the shadow zone.

A beam spreading via the lower troposphere refracts according to the refraction index gradient. As the refraction indexes change primarily with height, only the gradient of the vertical refraction index, n, is generally respected. If the refractivity height profile is linear, i.e., the refraction gradient is stable along the ray trajectory, then the transformation [3] considering a hypothetical Earth of effective radius R_e and linear ray trajectories can be used.

For calculation, the piecewise approximation of the surface is used in **Figure 2a**. The length of arc, r_B, and height, h_B, as shown in **Figure 2b**, are read. The coordinates (x_B, y_B) are provided by the subsequent equations [16]:

$$\begin{aligned} x_B &= (R_e + h_B)\sin\alpha_z \\ y_B &= (R_e + h_B)\cos\alpha_z - R_e \\ \alpha_z &= r_B/R_e. \end{aligned} \tag{7}$$

Obviously, an effect of these equations is greater when r_B and/or h_B are greater. This is demonstrated by examples in the next sections.

For a fast oscillating integrand, when the phase variation exceeds many times 2π, the utilization of usual trapezoidal or Simpson's quadrature formulas is inadequate. However, the numerical simulations (Eqs. (5) and (6)) may be performed by the generalized trapezoidal method [20], which is very efficient considering memory and CPU time. This method is based on the piecewise approximations of amplitudes as well as phases with equal intervals without any significant limitations. Numerical integrations of both real and imaginary parts are performed by usual trapezoidal method. It was found by numerous computations for various kinds of terrains that for frequencies less than 30 GHz, the integration steps may be 5–10 m [21].

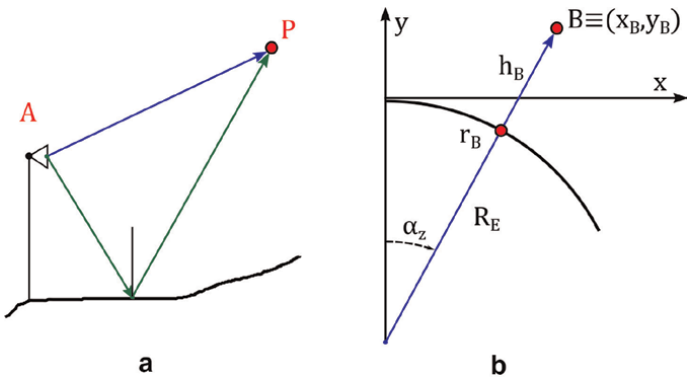

Figure 2.
(a) Earth surface and (b) curvature correction.

Actually, the usual requirement [9] that the spatial sampling resolution is less than λ/2 (1.5 cm for 10 GHz) is created mostly by aliasing.

However, for both analyses and syntheses, the simplified computation of the electrical field above an uneven earth [22], derived from above described method, could be used. This simplified method could compute Eqs. (5) and (6) using suitable simple approximations of Fresnel integrals. Clearly, the most important portions of piecewise approximations are in the vicinity of stationary phase points (i.e., points, where rays reflected from surfaces appear to come from mirror images). Therefore, the simplified method creates a more precise method than GO methods.

The difficulties of the described procedure are created by calculations used for the ground field. They may be reduced by using the physical theory of diffraction (PTD) [13, 24], which is a substantial expansion of PO. Furthermore, the novel variety of PTD [25] is acceptable for all scattering paths, particularly those that may contain forward scattering.

The normalized resulting field

$$A = 20\ \log|E(P)/E0|, \tag{8}$$

where $E(P)$ is the resulting field at P and $E0$ is the maximum incident electric field, which is determined for comparison of numerical simulations with experimental and other method data.

3. Radar coverage

A radar coverage diagram [3, 15, 26–30] comprises a volume inside in which the field is greater than the minimum useful value. The PEM models are very beautiful, but they ask for larger memories and CPU times, particularly for higher frequencies, elevation angles, and long ranges. Therefore diverse hybrid models have been produced by joining different models such as PEM and GO.

In the bistatic radar, unlike the monostatic radar, the transmitter and receiver are separated by a distance comparable to the target-to-receiver range [27]. The radar equation states

$$P_R = P_T G_T G_R \frac{f_T^2(\Phi,\Theta) f_R^2(\Phi,\Theta)\lambda^2\sigma_B}{(4\pi)^3 R_T^2 R_R^2 L_{TR}}, \tag{9}$$

where P_T, P_R are transmitted and received powers, G_T, G_R are transmitter and receiver antenna gains, f_T, f_R are transmitter and receiver antenna characteristics, λ is the wavelength of transmitted signal, σ_B is a radar cross section (RCS), and L_{TR} is loss on the transmitter-receiver path.

3.1 Monostatic radars

Usually vertical coverage diagrams are shown for free-space and plane ground effects, which consider a standard effective radius of $R_e = 8.5 \times 10^6$ m such as shown in **Figure 3**. This offers very useful qualitative ideas.

However, this approach is not quite satisfactory. Therefore, coverage diagrams of manufactured monostatic radars, which usually employ the same antenna for both transmitting and receiving antenna (i.e., $G_T = G_R$ and $f_T = f_R$), have been analyzed for numerous airports and radars, using the described PO method since the 1970s [31].

Figure 4 shows the new numerical simulations of electric fields for elevation angles, θ. The free-space and PO calculations of ground impacts for plane approximation of airport terrain profile as well as two effective radiuses (standard $R_e = 8.5 \times 10^6$ m and $R_e = 10.2 \times 10^6$ m) are compared. Even if it seems that these effective radiuses give very similar results, we should consider that the constant height contours of the coverage diagram curve downward as is shown in **Figure 3**.

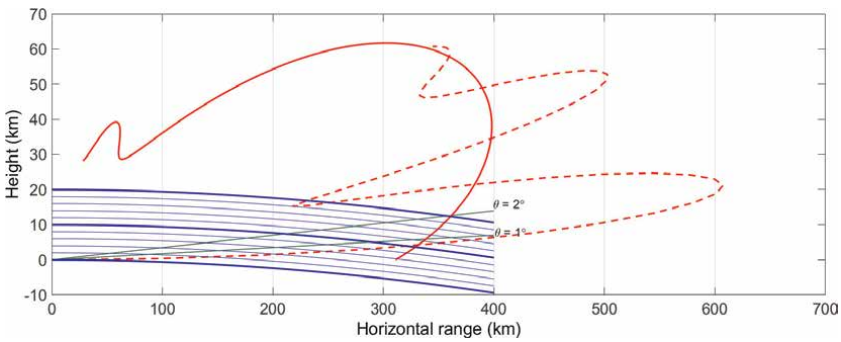

Figure 3.
Vertical coverage diagrams of radar for free-space (solid line) and ground effects.

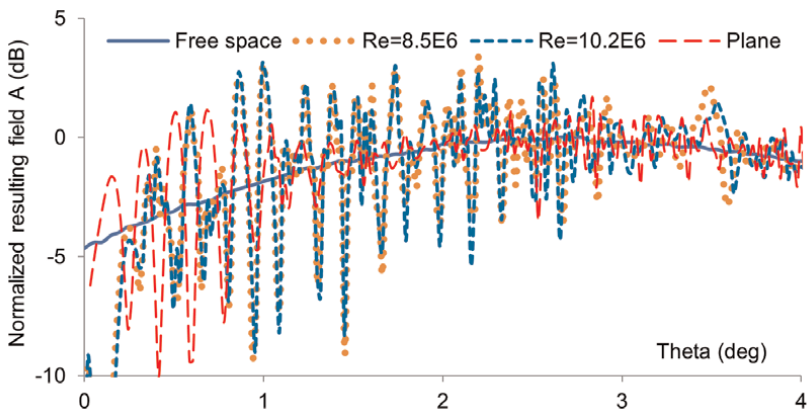

Figure 4.
Numerical simulations for free-space and PO calculations of ground impacts for plane approximation of airport terrain profile and two effective radiuses.

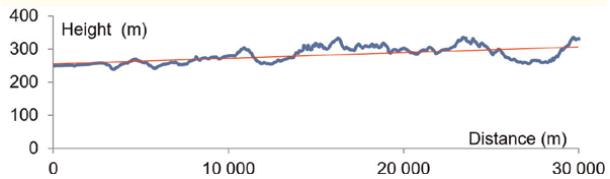

Figure 5.
Airport terrain profile with straight line fitting.

These simulations are performed for the novel radar development at an airport with terrain profile of a specified azimuth, displayed in **Figure 5**. We considered the surface with relative permittivity of ε_r = 2.9–0.044j and standard deviation of σ = 0 m for any part of the terrain.

However, this selection is not very important according to the detailed analyses [14, 15]. Obviously, a reflection-interference lobe pattern can be clearly seen. We used a straight line fitting shown in **Figure 5** for comparison. However, numerical simulations of plane approximation shown in **Figure 4** demonstrate a mere quality agreement, i.e., the plane approximation could be only used for a very rough calculation. This is due to fact that least squares data fittings, which seem very reasonable from mathematical point of view, use artificial slopes of terrain, especially for particular parts of surfaces.

On the other hand, calculations using the partial wave method [15, 32, 33] and mentioned simplified computations [22] correspond to PO simulations, even if we use a fit by eye for the set of data, because slopes of terrain correspond to piecewise approximations.

Obviously, the change of effective radius, R_e, is not usually substantial, especially for lower elevations. The used code for PO approximations allows only the utilization of one constant effective earth radius, R_e, for variable altitudes. This cannot be used for greater heights. However, the calculations of radar coverage could be more accurate using the recommendations ITU-R [34, 35] for the computations of refraction effects (estimation of the apparent elevation angle).

Experimental validations of vertical coverage calculations of radars are rather difficult as the RCS of various targets is usually extremely variable (obviously except conducting sphere). Usually, customers ask for confirmations of the radar coverage diagrams by test flights such as shown in **Figure 6**. However, that depends on several items such as air refraction effects and the RCS of the operated airplane, which are extremely changeable [27, 28, 36]. The RCS varies as a function of aspect angle and frequency (the period of the variability changes from seconds to a few tenths of a second). However, thanks to plentiful test flights made at different airports for changeable azimuths (therefore completely dissimilar topography profiles) and thorough analyses, we could state that PO simulations correspond to test flights.

The effective elevation pattern clearly depends on superposition of the direct propagating signal with reflecting signals. However, according to skills with operations and testing of radars nearby to airports with grassy vegetation, the diminishing of the reflection coefficient for angles up to 2° is not important [32]. We can conclude that the radar coverage diagram of certain specific monostatic radar could be very useful as neighboring terrains of radar sites are usually very similar, and therefore it could be considered as a typical case.

3.2 Bistatic radars

There are several competitive signals reducing the maximum range and complicating the signal processing. They are the direct signal, correlated reflections of

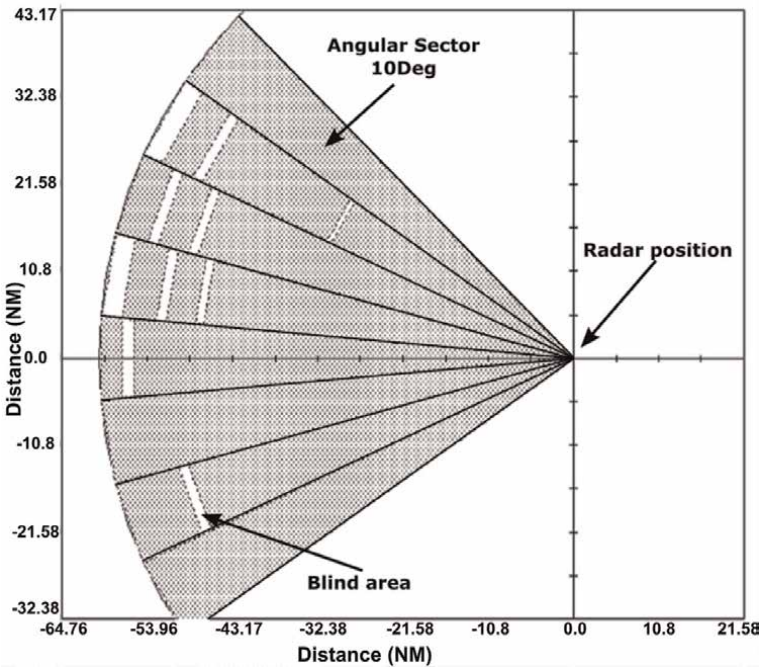

Figure 6.
Test flight.

terrain objects (clutter), non-correlated signals transmitted by other sources at the same frequency (electromagnetic noise), and the thermal noise. Clearly, the investigation of bistatic radars and especially passive coherent locator (PCL), which uses transmitters of opportunity such as FM radio broadcasting, is very complicated [27, 37, 38].

As the transmitter and receiver are separated, the ground effects should be analyzed independently. That means, the propagation above the terrain between transmitter(s) and target and receiver(s) and target must be examined. This case is much more complicated than monostatic radar. However, **Figure 3** could be very useful for investigation of bistatic radars for various different situations. Moreover, PO modeling very easily permits the typical configuration calculations for transmitters of opportunity.

Obviously, the bistatic RCS should be also investigated. Usually, a bistatic RCS is lower than the monostatic RCS measured on the bisector of complicated targets. However, some target aspect angles can generate a low monostatic RCS and high bistatic specular RCS. A limiting case of the bistatic geometry occurs when the target is on the transmitter-receiver baseline. A considerable improvement of scattering can be generated, as the forward scatter RCS, σ_f, is approximately

$$\sigma_f = 4\pi S^2/\lambda \tag{10}$$

where S is the target projected area and λ is a transmitted wavelength even for stealth targets with ideally absorbing surfaces [27].

4. Antenna far-field measuring ranges

We measure an antenna under test (AUT) on an antenna range [39–41]. The plane wave of uniform amplitude and phase is an ideal situation for measuring of

far-field electromagnetic wave features of the AUT. This wonderful situation is not realizable. However, it can be roughly made, if we use a large separation between the AUT and the transmitting (or receiving) antenna at an outdoor range. When we enlarge the separation, the spherical phase-front becomes more planar over the AUT aperture. When the separation equals $2D^2/\lambda$, where D is the largest diameter of the AUT, then the maximum phase error is about 22.5°.

Furthermore, reflections from the ground and adjacent objects could erroneously affect the AUT illuminations. Apparently, the electromagnetic field quality of the quiet zone depends on AUT features. Thus, numerical simulation analyses are very motivating. Applicable suppression of reflected signals should be done by a combination of line-of-sight clearance, transmitter and/or receiver antenna directivities, and sidelobe suppression. Perhaps, range ground screening could also be considered.

The proposed PO method [18] analyzes the illuminated part of terrain and abrupt change of height, which create the shadowed part. Naturally, the utilization of knife-edge diffraction and Fock's spherical surface solutions, which neglect terrain imperfections, creates only approximate solutions. However, the comparison shows that the PO method produces acceptable results, as this method actually replaces a real scattering object by the equivalent currents. Moreover, problems may be reduced by using the physical theory of diffraction [24, 25].

Obviously, a smaller AUT asks for a smaller quiet zone, but spurious signal suppressions by the AUT could be very poor. On the contrary, a larger AUT requires a larger quiet zone, but spurious signal suppressions by the AUT could be much improved.

We could test the function of any antenna through concrete solid angles and frequency bands. The antenna features are typically quantified by the requests of operating systems and describe areas where they are significant. Plentiful measurements have been obtained thanks to thorough tests of the far-field ranges for different situations since the early 1970s (as for any original antenna type, the vertical range illumination was tested). Obviously, any discrepancies and changes have been comprehensively analyzed to discover the possible reasons of those effects.

Of course, the effect of terrain on scattering field is very important. But, the numerous technical and economic issues such as possibilities of electrical power supply, roads suitable for tested antenna transport, effect of nearby objects (buildings, woods), electromagnetic interference sources, expenses, and total budget should be considered. Therefore, various sites have been thoroughly analyzed. In fact, the program [14] was proposed for different studies of projected and/or built far-field ranges.

Therefore, we present the novel comparison with different relative permittivity values ε_r and standard deviations σ in **Figure 7** for the profile shown in **Figure 8**. The $h = 0$ height corresponds to upper positioner placed on the tower.

The simulations of dry ground of $\varepsilon_r = 3.2–0.015j$ and wet ground of $\varepsilon_r = 30–2.5j$ are shown. It can be seen that the results are nearly the same. Experimental values and numerical simulations were performed with a transmitting reflector diameter of $D = 3$ m. To validate the influence of greater beam width, the computations with the reflector diameter of $D = 0.6$ m ($\varepsilon_r = 30–0.02j$) are also presented. Clearly, standard deviations σ of random surface deviations are more significant, especially for larger beam width (i.e., $D = 0.6$ m).

The problems of ground scattering could be diminished by using fences, which could be very demanding [40]. The diffraction fences on the range can reduce the level of reflections. However, the fences inevitably introduce disturbances in the incident field due to diffraction effects along their wedges. Therefore, a practical

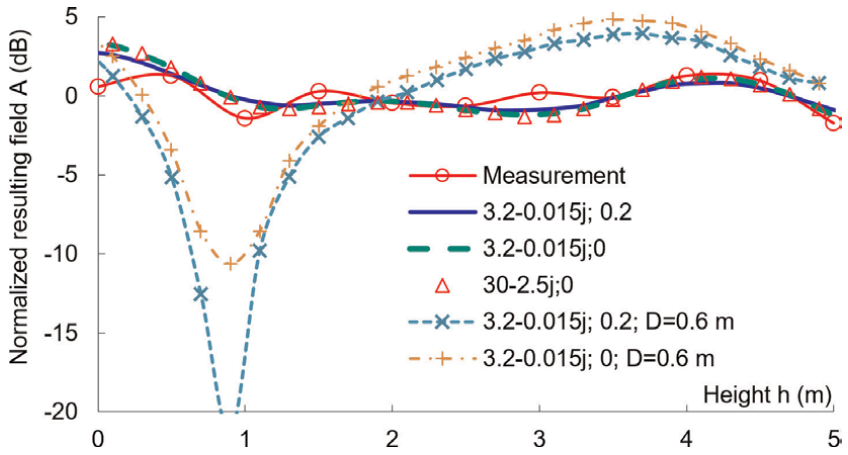

Figure 7.
Measurement, numerical simulations for ε_r = 30–2.5j and ε_r = 3.2–0.015j, ground standard deviations of σ = 0.2 m and σ = 0 m, and calculations with reflector diameter of D = 0.6 m for ε_r = 3.2–0.015j, and ground standard deviations of σ = 0.2 m and σ = 0 m.

fence proposal is a compromise between reflection reductions and residual diffraction. Of course, it has been shown [18] that Eqs. (5) and (6) may be utilized for computation of both illuminated and shadow radiation considering the polarizations even for the shadow zone. That is numerical simulations may be performed for greater as well as lower heights without any artificial combinations of different methods. Considering the complex Fresnel integral [1] and Eq. (2), the Cornu spiral derived from straight-edge diffraction can be applied. Therefore, the length of reflected rays shown in **Figure 8** could be very useful for fence design.

Wedge diffractions of fences could be diminished using tuned slots (which are effective at a single frequency but are frequency sensitive) or serrations along the edge. Both approaches ask for structures which expand several wavelengths above the edge. The most understandable design is to maintain low-level illumination of the fence edge, if possible. That sometimes leads to the low multiple-fence design with proper tilting. However, usually one to three fences are used.

Generally, the differences between measuring, when the probe (small horn antenna) is moved between h = 0 and h = 5 m, and calculations may be partially clarified considering reflective coefficient variations and scattering from objects, which are nearby the positioner. Such objects include a tower construction and safeguard bars.

The reflective coefficients fluctuate due to seasonal ground circumstances as the ground may be overgrown by plants, coated by snow or farmed. They influence both scattered and resulting fields. They are not frequently significant for low

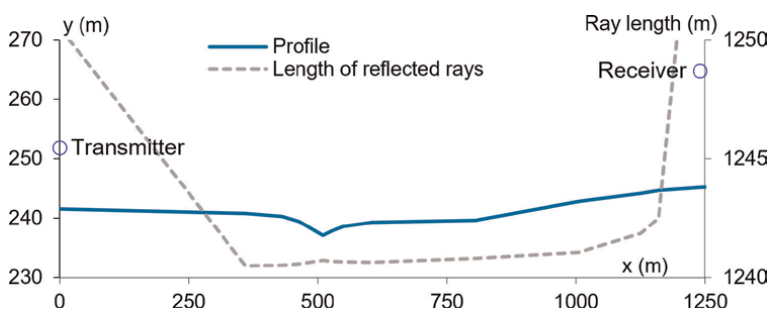

Figure 8.
Profile of far-field range and the length of reflected rays.

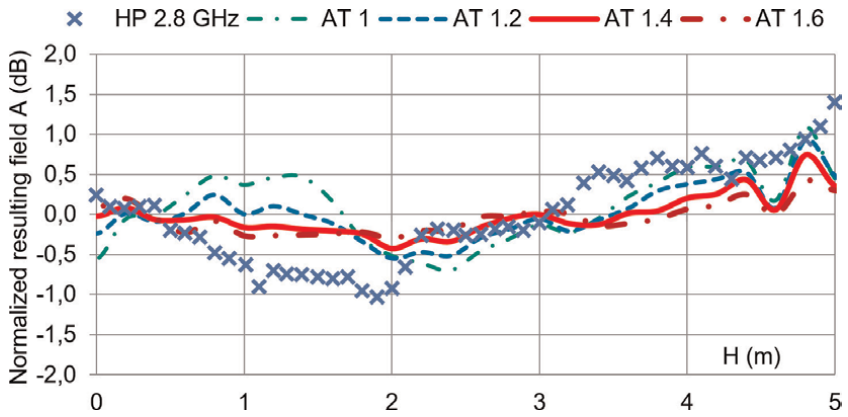

Figure 9.
The comparison of measurements with antenna tilt 1.4° (HP 2.8 GHz) and calculations of normalized resulting field for frequency of 2.8 GHz and the antenna tilt of 1° (AT 1), 1.2° (AT 1.2), 1.4° (AT 1.4), and 1.6° (AT 1.6).

random deviations, as the local reflections are nearly equal to −1 for low grazing angles irrespective of polarization. However, **Figure 7** shows that larger ground deviations may influence the measured values more significantly. Site tests and numerous computations since the 1970s validate these data. Moreover, the experiments and computations have been done with various ranges with quite different terrain profiles. Various initial and reconstructed towers, different transmitter antennas (such as prime focus and dual-reflector Cassegrain antennas with smooth-wall or conical corrugated horns), and several types of probes are used for both linear and elliptical polarizations and frequency bands.

Actually, the results fluctuate during seasons and due to location of auxiliary equipment (including occasionally crane). The experiments show that reflection coefficients of antenna ranges are diminished in summer, when a terrain is covered by wheat or other vegetations for frequency bands of 1 up to 10 GHz.

Numerical simulations have been used both for design and optimizing of the rebuilt antenna range [14–18, 36, 39, 42]. **Figure 9** shows the comparison of measurements with antenna tilt 1.4° (horizontal polarization HP 2.8 GHz) and calculations of normalized resulting field A (dB), using the horizontal polarization and frequency of 2.8 GHz. Various antenna tilts of 1° (AT 1), 1.2° (AT 1.2), 1.4° (AT 1.4), and 1.6° (AT 1.6) are analyzed. It is quite clear that experimental optimizing, when we consider the antenna tilt as well as frequencies, polarizations, and random deviations, is very time-consuming. Therefore, numerical simulations are extremely useful. They could discover quite new phenomena and create new concepts.

Obviously, numerical simulations have been analyzed considering disturbing effects of various obstacles such as nearby constructions, trees, and changeable surface. This is important especially for bigger random deviations, i.e., the surface standard deviation, σ.

5. Effects of air refraction index

Electromagnetic wave propagation in the troposphere varies according to the air refractive index [3, 5, 34, 35]. The various experimental analyses of radio-wave characteristics and atmospheric refracting "N unit" layers have been already published such as [43–46]. All these factors can be used for calculation. The enduring testing of physical tropospheric features were made at the receiving site on a

tower with 19 different elevations from 5 m up to 147 m with mean extent spans of about 7.5 m. Simultaneously, the five receiving 0.65 m dishes at several elevations measured the electromagnetic field in the troposphere with the link length of R_0 = 49.8 km. Bearing in mind the 1-day measuring of refracting N units, **Figures 10** and **11** show the comparison of measurements and PO computations.

Figure 10 shows the spreading of measured values during the same day denoted by MEAS.MAX and MEAS.MIN, which show measured maxima and minima. Comparisons of maxima and minima of measurements during a day with PO numerical simulations of 0.65 m diameter antenna, surface with ε = 15–3.5j, σ equals to 0 or 0.2 m, and standard $R_e = 8.5 \times 10^6$ m reveal that the simulations using only one R_e cannot be used for a fine modeling. Even if we use $R_e = 6.9 \times 10^6$ m, which correspond to height of 51 m, the problem is not resolved for several heights. Therefore the other approach should be used.

The observation of refractive index distributions, for various heights during the same day, reveals that distributions are very changeable. Therefore, we cannot speak correctly about stratum formulation. Nevertheless, we select the same R_e effective radiuses for individual "layers" for 11 AM. The heights of 51, 61, 90, 120, and 145 m correspond to PO simulations with individual R_e selections for each height ("layer"). Therefore the small parts of graphs are only displayed in **Figure 11**.

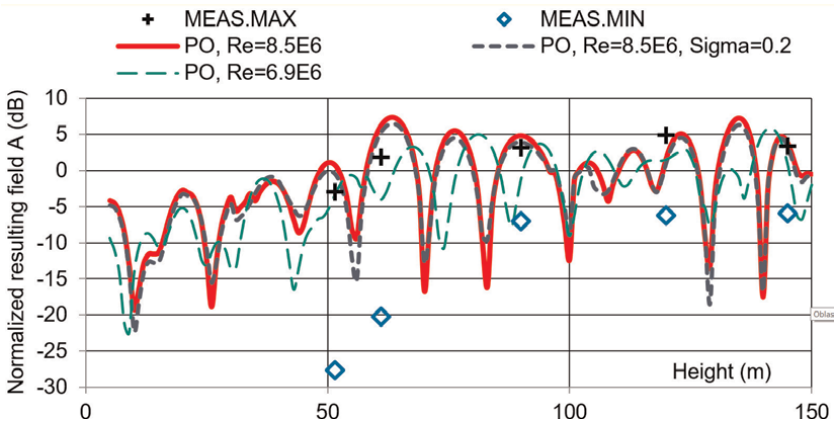

Figure 10.
Comparison of measurements, where MEAS.MAX and MEAS.MIN are maxima and minima during a day, with the 0.65 m diameter and standard $R_e = 8.5 \times 10^6$ m (with σ equals to 0 or 0.2 m) and $R_e = 6.9 \times 10^6$ m for PO numerical simulations.

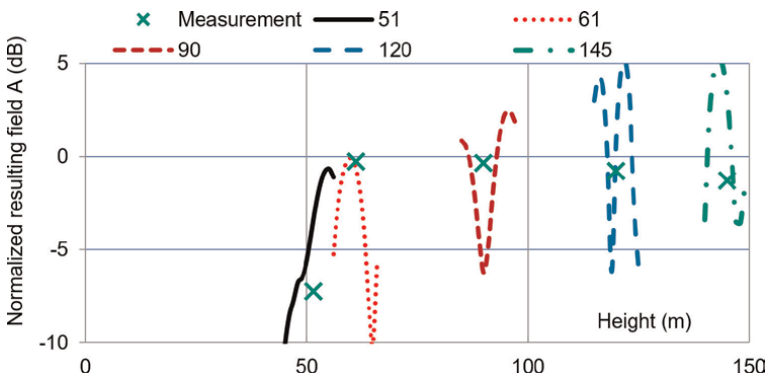

Figure 11.
Comparison of measurements with 0.65 m diameter for PO numerical simulations for heights of 51, 61, 90, 120, and 145 m.

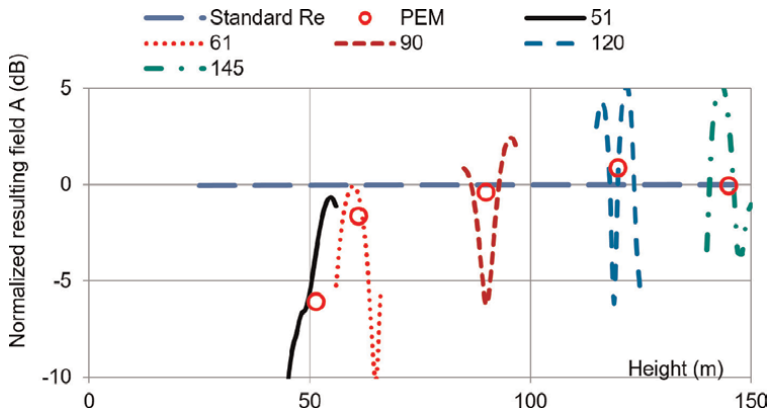

Figure 12.
Comparison of the standard R_e (without ground reflections), PEM, and PO numerical simulations for heights of 51, 61, 90, 120, and 145 m.

This demonstrates that the described PO method may offer reliable calculations of three-dimensional spreading of refraction.

Considering the 1-day measuring of refracting N units, **Figure 12** shows the comparison of computations using PO and PEM for 11 AM (i.e., the same time as in **Figure 11**). It can be seen that PO and PEM provide similar results, if we select the same R_e effective radiuses for individual "layers" (both for PEM and PO as correspond to the "measurement" values). The standard R_e shows calculations without ground reflections. Clearly, the effects of the antenna radiation pattern are negligible for low elevations.

The PEM has been expansively examined. Evaluation of experiments and numerical simulations using the PEM revealed that PEM simulations correspond mostly to measurements when a particular vertical gradient may be used. However, a simulation of multipath spreading for extremely confused circumstances was unacceptable. Unfortunately, the requirement that not less than three frequencies should be used at the same time to offer an obvious correspondence with theory [3] has not been accomplished as frequency of 10.671 GHz was only used. Using the PO method, the influence of refracting indexes was examined infrequently, and initial situations have been only announced [4, 6]. Therefore, new comparisons are performed.

However, the employed code for PO approximations allows only the utilization of one constant effective earth radius, R_e, for variable altitudes.

Using the code [18, 19] we could use different electrical parameters for any ground fragment. In spite of this, the detailed characteristics of the ground are not identified. In fact, they are not stationary and may change very rapidly. Thus, ε_r = 15–3.5j is only employed for computations of air refraction index influences.

6. Conclusions

This chapter briefly describes the PO approximation, which is frequently utilized. The novel comparisons using recent PO method are presented for measurements and numerical simulations. We have investigated experimentally different ground situations and variations of plants, snow, winter, or summer through plentiful years for different frequency bands and polarizations.

We analyze radar coverage diagrams considering the usual monostatic radars as well as bistatic radars. We can conclude that the radar coverage diagram of certain

specific monostatic radar could be very useful as neighboring terrains of radar sites are usually very similar. Therefore, it could be considered as a typical case. Analyses of bistatic radars are difficult as the propagation above the terrain between transmitter(s) and target and receiver and target must be analyzed. This case is much more complicated comparing with monostatic radar. However, **Figure 3** could be very useful for investigation of bistatic radars for various different situations. Moreover, considering passive coherent locators, the PO modeling permits typical configuration calculations for various transmitters of opportunity.

The measuring antenna far-field range (relatively short distance about 1 km) shows generally that the differences between measuring, when the probe (small horn antenna) is moved between $h = 0$ and $h = 5$ m, and calculations may be partially clarified. We have considered reflective coefficient variations due to plants, snow, winter, or summer and scattering from auxiliary objects, which are nearby the positioner. Such objects include tower assemblies and different safeguard obstructions. The utilization of diffraction fences is briefly explained. Numerical simulations have been successfully used both for design and optimizing of the rebuilt antenna range.

The observation of refractive index distributions for distance of 49.8 km, for various heights during the same day, reveals that distributions are very changeable. Therefore, we cannot speak correctly about stratum formulation. Nevertheless, we select for individual "layers" of PO simulations the same R_e effective radiuses, which were used for PEM simulations. Therefore the small parts of graphs are only displayed for comparison with measurements and PEM simulations.

It has been validated that the upgraded PO method offers more trustworthy calculations for low elevation propagations and diffraction zones. In this method, there is no supporting technique for special tropospheric situations for data transmission and communications together with electromagnetic compatibility. The small discrepancies could be incompletely clarified since permittivity, conductivity, and standard deviation change. Obviously, the selection of suitable effective radiuses, R_e, for individual heights could substantially diminish these discrepancies that could be very useful both for syntheses and analyses of various propagation phenomena including refraction and reflection from uneven ground. Obviously, this method provides more thoughtful results, when beams are narrow in horizontal plane such as pencil- or fan-shaped, which are used in radars.

The described PO method provides reliable computations for low-height fields and diffraction zones for numerous uneven terrains and realistic refractive index spreading. The used code for PO approximations allows only the utilization of one constant effective earth radius, R_e, for variable altitudes. This cannot be used for greater heights. Effects of the air refraction index, studied in part 5, could be neglected for coarse numerical simulations. However, the calculations could be more accurate using the recommendations ITU-R for higher altitudes of large-scale refractive effects.

Frequently, refractive propagation effects on electromagnetic wave propagation could be neglected especially for lower elevations. It is clearly demonstrated that we should consider ground scattering and we cannot only analyze the radiation pattern, refraction, and tropospheric losses.

Acknowledgements

The authors thank deceased Dr. D. Kupcak for very beneficial ideas during longtime collaboration both from theoretical and practical viewpoints.

The work was supported from ERDF/ESF "Cooperation in Applied Research between the University of Pardubice and companies, in the Field of Positioning, Detection and Simulation Technology for Transport Systems (PosiTrans)" (No. CZ.02.1.01/0.0/0.0/17_049/0008394).

Author details

Vladimir Schejbal*, Ondrej Fiser and Vadim Zavodny
University of Pardubice, Pardubice, Czech Republic

*Address all correspondence to: vladimir.schejbal@upce.cz